Coherent and incoherent ultrasound backscatter from cell aggregates

Romain de Monchy
Aix-Marseille Université, Centre National de la Recherche Scientifique, Centrale Marseille,
Laboratoire de Mécanique et d'Acoustique, 4 Impasse Nikola Tesla, CS 40006,
13453 Marseille cedex 13, France

François Destrempes
Laboratory of Biorheology and Medical Ultrasonics, University of Montreal Hospital Research Centre
(CRCHUM), 900 St-Denis, Suite R11.720, Montreal H2X 0A9, Canada

Ratan K. Saha
Department of Applied Sciences, Indian Institute of Information Technology Allahabad, Jhalwa, Devghat,
Allahabad 211012, India

Guy Cloutier[a]
Laboratory of Biorheology and Medical Ultrasonics, University of Montreal Hospital Research Centre
(CRCHUM), 900 St-Denis, Suite R11.720, Montreal H2X 0A9, Canada

Emilie Franceschini[b]
Aix-Marseille Université, Centre National de la Recherche Scientifique, Centrale Marseille,
Laboratoire de Mécanique et d'Acoustique, 4 Impasse Nikola Tesla, CS 40006,
13453 Marseille cedex 13, France

The effective medium theory (EMT) was recently developed to model the ultrasound backscatter from aggregating red blood cells [Franceschini, Metzger, and Cloutier, IEEE Trans. Ultrason. Ferroelectr. Freq. Control **58**, 2668–2679 (2011)]. The EMT assumes that aggregates can be treated as homogeneous effective scatterers, which have effective properties determined by the aggregate compactness and the acoustical characteristics of the cells and the surrounding medium. In this study, the EMT is further developed to decompose the differential backscattering cross section of a single cell aggregate into coherent and incoherent components. The coherent component corresponds to the squared norm of the average scattering amplitude from the effective scatterer, and the incoherent component considers the variance of the scattering amplitude (i.e., the mean squared norm of the fluctuation of the scattering amplitude around its mean) within the effective scatterer. A theoretical expression for the incoherent component based on the structure factor is proposed and compared with another formulation based on the Gaussian direct correlation function. This theoretical improvement is assessed using computer simulations of ultrasound backscatter from aggregating cells. The consideration of the incoherent component based on the structure factor allows us to approximate the simulations satisfactorily for a product of the wavenumber times the aggregate radius kr_{ag} around 2. © *2016 Acoustical Society of America*. [http://dx.doi.org/10.1121/1.4962502]

[GH]

Pages: 2173–2184

I. INTRODUCTION

Ultrasound scattering from biological tissues exhibits a frequency dependence which is related to the structure of the insonified medium. For determining the tissue microstructure, one approach consists in fitting the measured frequency-dependent backscatter coefficient (BSC) to a theoretical BSC derived using an appropriate theoretical scattering model. Two theoretical scattering models are often used in the field of quantitative ultrasound (QUS) imaging.

The first model, named the spherical Gaussian model, describes a tissue as a random inhomogeneous continuum with impedance fluctuations.[1] The second model, named the fluid sphere model, considers tissue as randomly distributed discrete scatterers with impedance differing from a homogeneous background medium, where the cells are generally considered as the dominant source of scatterers and modeled as fluid spheres.[2] In both models, the scatterers are assumed to be independently and uniformly randomly distributed, which may correspond to the case a low scatterer concentration, such that each scatterer individually contributes to the backscattered power. As a result, the BSC is proportional to the scatterer number density. This relationship has been used to compute the estimates of scatterer size and concentration.

[a]Also at: Department of Radiology, Radio-Oncology and Nuclear Medicine, and Institute of Biomedical Engineering, University of Montreal, Montreal H3T IJ4, Canada.
[b]Electronic mail: franceschini@lma.cnrs-mrs.fr

However, biological tissues often have high cellular concentrations and complex structures that invalidate the assumption of those models.[3,4] For example, some tumors have densely packed cells and eventually aggregating cells such as breast sarcoma.[5] Blood contains a high volume fraction of red blood cells (RBCs) between 30% and 50% that form aggregates having linear structures (termed *rouleaux*) in normal blood or clumps in some pathologies, as in diabetes mellitus.[6,7] Therefore, theoretical scattering models have been proposed to include high cellular concentration together with aggregating cells, and to estimate scatterer structures.[8,9] A scattering model called the effective medium theory combined with the structure factor model (EMTSFM) was recently proposed.[10] In this model, the aggregates of cells are viewed as individual scatterers which have effective properties determined by the aggregate compactness and the acoustical characteristics of the cells and the surrounding medium. The approximation of cell aggregates as homogeneous effective scatterers is combined with the structure factor model to consider the concentrated medium, i.e., to consider the interference effects caused by the correlations between the spatial positions of effective scatterers. The EMTSFM allows characterization of the radius and of the compactness of cell aggregates, as shown in a previous simulation study.[11]

The goal of the current study was to further develop the EMTSFM and to extend its validity into a larger frequency range. In that aim, the effective medium theory (EMT) was modified to decompose the differential backscattering cross section of a single cell aggregate into coherent and incoherent components as proposed by Morse and Ingard.[12] The coherent component corresponds to the squared norm of the average scattering amplitude from the effective scatterer, and the incoherent component considers the variance of the scattering amplitude (i.e., the mean squared norm of the fluctuation of the scattering amplitude around its mean) within the effective scatterer. Note that only the coherent component was taken into account in our previous works.[10,11] A new theoretical expression for the incoherent component based on the structure factor is proposed. This theoretical improvement was assessed using three-dimensional (3D) computer simulations of ultrasound backscatter from aggregating RBCs. The new incoherent component based on the structure factor was compared to the incoherent component based on a Gaussian direct correlation function proposed by Morse and Ingard.[12]

II. THEORY

In this section, the theoretical expression for the ultrasound backscattering response from one aggregate of cells is proposed. Then, the theoretical BSC expression for an ensemble of identical aggregates that was developed in Ref. 10 is briefly recalled.

A. Differential backscattering cross-section σ_{ag} of one aggregate of cells

In the present paper, we consider identical cells distributed randomly inside an aggregate. It is assumed that the

incident wavelength is large compared to the cell size. Consequently, the cell shape can be approximated by a sphere of radius a having an equivalent volume $V_c = (4/3)\pi a^3$. Cells are described in terms of their mass density ρ_c and compressibility κ_c, and their surrounding medium is characterized by a mass density ρ_0 and a compressibility κ_0. The cells are assumed to have small fluctuations in acoustic parameters[4,9] such that multiple scattering is neglected in line with the Born approximation. An aggregate of cells, denoted V_{ag}, is assumed to be spherical as it occurs in some tissues (e.g., RBC aggregates in pathological cases[6,7] or breast sarcoma tumors[5]). Assuming that the distance from V_{ag} to the point of observation is much larger that the dimensions of V_{ag} (i.e., far-field approximation), the backscattered wave pressure from an aggregate is expressed in terms of the backscattered amplitude Φ_{ag}, i.e., $p_s(\mathbf{r}) = (e^{ikr}/r)\Phi_{ag}(k)$, with[13]

$$\Phi_{ag}(k) = \frac{k^2}{4\pi} \int_{\mathbf{V}_{ag}} \left[\gamma_\kappa(\mathbf{r}_0) - \gamma_\rho(\mathbf{r}_0) \right] e^{2ik\mathbf{n_0}\cdot\mathbf{r}_0} \, d^3\mathbf{r}_0,$$

where k is the wavenumber, $\mathbf{r}_0$ is the position in the 3D space, $\mathbf{n}_0$ is the incident wave direction, $\gamma_\kappa(\mathbf{r}_0) = (\kappa(\mathbf{r}_0) - \kappa_0)/\kappa_0$, and $\gamma_\rho(\mathbf{r}_0) = (\rho(\mathbf{r}_0) - \rho_0)/\rho(\mathbf{r}_0)$ are the fractional variations in compressibility and mass density, respectively. One has

$$\gamma_\kappa(\mathbf{r}_0) - \gamma_\rho(\mathbf{r}_0) = \begin{cases} \gamma_\kappa - \gamma_\rho & (\text{if } \mathbf{r}_0 \text{ is inside the cells}), \\ 0 & (\text{if } \mathbf{r}_0 \text{ is outside the cells}), \end{cases}$$

(1)

where $\gamma_\kappa = (\kappa_c - \kappa_0)/\kappa_0$ and $\gamma_\rho = (\rho_c - \rho_0)/\rho_c$. Assuming N identical cells inside an aggregate with centers located at positions $\mathbf{r}_j, j = 1, ..., N$, and considering the change of variable $\mathbf{r}'_0 = \mathbf{r}_0 - \mathbf{r}_j$, the scattering amplitude can be expressed as

$$\Phi_{ag}(k) = \frac{k^2(\gamma_\kappa - \gamma_\rho)}{4\pi} V_c \left(V_c^{-1} \int_{\mathbf{V}_a} e^{2ik\mathbf{n_0}\cdot\mathbf{r}'_0} d^3\mathbf{r}'_0 \right) \sum_{j=1}^{N} e^{2ik\mathbf{n_0}\cdot\mathbf{r}_j},$$

(2)

where $\mathbf{V}_a$ is a sphere of radius a centered at the origin (see Appendix A for details). The integral term in Eq. (2) is equal to

$$V_c^{-1} \int_{\mathbf{V}_a} e^{2ik\mathbf{n_0}\cdot\mathbf{r}'_0} d^3\mathbf{r}'_0 = \left(\frac{3\left(\sin(2ka) - 2ka\cos(2ka)\right)}{(2ka)^3} \right)$$
$$= F_0(k;a),$$

(3)

and $F_0(k;a)^2 = F(k;a)$ is the fluid-sphere form factor.[13] From there, the scattering amplitude resulting from one aggregate is expressed as

$$\Phi_{ag}(k) = \frac{k^2(\gamma_\kappa - \gamma_\rho)}{4\pi} V_c F_0(k;a) \sum_{j=1}^{N} e^{2ik\mathbf{n_0}\cdot\mathbf{r}_j}.$$

(4)

As previously studied by Morse and Ingard,[12] the differential backscattering cross-section σ_{ag} of an aggregate is computed as the sum of two components

$$\sigma_{ag} = \sigma_{ag,coh} + \sigma_{ag,inc}, \tag{5}$$

where the coherent component $\sigma_{ag,coh}$ is the squared norm of the average scattering amplitude, and the incoherent component $\sigma_{ag,inc}$ describes the mean squared norm of the fluctuation of the scattering amplitude around its mean (i.e., the variance of the scattering amplitude), as detailed below.

1. The coherent component

The coherent component of the differential backscattering cross-section is obtained from the coherent scattering amplitude as

$$\sigma_{ag,coh}(k) = |\langle \Phi_{ag}(k) \rangle|^2,$$

where $\langle \cdots \rangle$ represents the expected value of a random variable. One computes

$$\langle \Phi_{ag}(k) \rangle = \frac{k^2(\gamma_\kappa - \gamma_\rho)}{4\pi} V_c F_0(k;a) \sum_{j=1}^{N} \langle e^{2ik\mathbf{n}_0 \cdot \mathbf{r}_j} \rangle$$

$$= \frac{k^2(\gamma_\kappa - \gamma_\rho)}{4\pi} \phi_i V_{ag} F_0(k;a) \frac{1}{N} \sum_{j=1}^{N} \langle e^{2ik\mathbf{n}_0 \cdot \mathbf{r}_j} \rangle, \tag{6}$$

where $V_{ag} = (4/3)\pi r_{ag}^3$ is the volume of an aggregate of radius r_{ag}, and $\phi_i = NV_c/V_{ag}$ is the aggregate compactness. Next, we define

$$\rho_{ag} = [\phi_i/\rho_c + (1-\phi_i)/\rho_0]^{-1},$$
$$\kappa_{ag} = \phi_i \kappa_c + (1-\phi_i)\kappa_0, \tag{7}$$

which are obtained from the average values of $1/\rho$ and κ, respectively, within the aggregate, as mentioned in Eq. (8.2.23) of Morse and Ingard.[12] Denoting $\gamma_{\kappa,ag} = (\kappa_{ag} - \kappa_0)/\kappa_0$ and $\gamma_{\rho,ag} = (\rho_{ag} - \rho_0)/\rho_{ag}$, one computes $(\gamma_\kappa - \gamma_\rho)\phi_i = \gamma_{\kappa,ag} - \gamma_{\rho,ag}$. Based on these definitions, it follows that the coherent scattering amplitude of the aggregate is expressed as

$$\langle \Phi_{ag}(k) \rangle = \frac{k^2(\gamma_{\kappa,ag} - \gamma_{\rho,ag})}{4\pi} V_{ag} F_0(k;a) \frac{1}{N} \sum_{j=1}^{N} \langle e^{2ik\mathbf{n}_0 \cdot \mathbf{r}_j} \rangle. \tag{8}$$

Note that in this derivation, no approximation was used, but rather algebraic manipulations and definitions.

The expression $\mathcal{F}_{coh}(k) = F_0(k;a) 1/N \sum_{j=1}^{N} \langle e^{2ik\mathbf{n}_0 \cdot \mathbf{r}_j} \rangle$ corresponds to the Fourier transform of the function $\langle 1/N \sum \chi_a(\mathbf{r} - \mathbf{r}_j) \rangle$ that describes a system of spheres, where $\chi_a(\mathbf{r} - \mathbf{r}_j) = 1$ inside a sphere $\mathbf{V}_a$ of radius a centered at $\mathbf{r}_j$, and 0 elsewhere. Since it is not straightforward to compute the expression $\mathcal{F}_{coh}(k)$, we approximate this quantity with the expression $F_0(k,r')$ given in Eq. (3) for an equivalent full sphere of radius r'. The full sphere choice was motivated here by the postulated spherical distribution of cells in

aggregates. In order to match the low frequency approximations of the scattering amplitudes from the system of spheres and from the equivalent full sphere, their gyration radii R_g should be equal. The gyration radius of an object corresponds to the root mean square distance of the object's points from its center of mass. In the case of a system of N spheres of radius a, the gyration radius is equal to

$$R_g = \sqrt{\frac{3}{5}a^2 + \frac{1}{N}\sum_{j=1}^{N} |\mathbf{r}_j|^2}, \tag{9}$$

where $\mathbf{r}_j$ is the position vector of the jth cell with respect to the aggregate center, as given in Eq. (6) of Saha et al.[14] So, the radius r' of the equivalent full sphere must be expressed as $r' = \sqrt{5/3}R_g$, as demonstrated in Appendix B. Henceforth, from Eq. (8), the coherent scattering amplitude resulting from one aggregate is approximated as

$$\langle \Phi_{ag}(k) \rangle \approx \frac{k^2(\gamma_{\kappa,ag} - \gamma_{\rho,ag})}{4\pi} V_{ag} F_0\left(k; \sqrt{\frac{5}{3}}R_g\right). \tag{10}$$

All together, the coherent component of the differential backscattering cross-section is modeled as

$$\sigma_{ag,coh}(k) \approx \frac{k^4(\gamma_{\kappa,ag} - \gamma_{\rho,ag})^2}{16\pi^2} V_{ag}^2 F\left(k; \sqrt{\frac{5}{3}}R_g\right). \tag{11}$$

One should note that in the former work,[10] the fluid-sphere form factor F given in Eq. (11), was computed by considering the external radius of the aggregate r_{ag} (instead of $\sqrt{5/3}R_g$ in the present work). Comparison between the former and the present coherent form factors will be presented in the Sec. IV A.

2. The incoherent component

Inside an aggregate, each cell produces a scattered wave as a sphere of radius a, with density ρ_c and compressibility κ_c, in a surrounding medium of density ρ_0 and compressibility κ_0 throughout the aggregate. But since the density and compressibility of the corresponding effective scatterer are equal to ρ_{ag} and k_{ag}, respectively, the ratio of the speed of sound in the surrounding medium to the average speed of sound within the aggregate is equal to $\sqrt{\rho_{ag}\kappa_{ag}}/\sqrt{\rho_0\kappa_0}$. Due to this diffraction phenomenon, the wavenumber accounting for the acoustical inhomogeneities within an aggregate is modified as[12] $k_{ag} = k\sqrt{\rho_{ag}\kappa_{ag}}/\sqrt{\rho_0\kappa_0}$. Based on Eq. (4), the incoherent component of the differential backscattering cross-section is equal to

$$\sigma_{ag,inc}(k) = \langle |\Phi_{ag}(k_{ag}) - \langle \Phi_{ag}(k_{ag}) \rangle|^2 \rangle \tag{12}$$

$$= \frac{k_{ag}^4(\gamma_\kappa - \gamma_\rho)^2}{16\pi^2} V_c^2 N F(k_{ag};a) S_0(k_{ag};a,\phi_i), \tag{13}$$

where

J. Acoust. Soc. Am. **140** (3), September 2016

de Monchy *et al.*   2175

$$S_0(k; a, \phi_i) = \left\langle \frac{1}{N} \left| \sum_{j=1}^{N} e^{2ik\mathbf{n_0 \cdot r}_j} - \sum_{j=1}^{N} \langle e^{2ik\mathbf{n_0 \cdot r}_j} \rangle \right|^2 \right\rangle \quad (14)$$

is the structure factor for a collection of N randomly distributed identical spheres of radius a and of concentration ϕ_i within an aggregate. Assuming that the aggregate is sufficiently large, Eq. (14) corresponds to Eq. (10) in Ref. 15. This latter structure factor was analytically calculated as established by Wertheim,[16] which is denoted here by $S(k_{ag}; a, \phi_i)$. One thus obtains the expression

$$\sigma_{ag,inc}(k) \approx \frac{k_{ag}^4 (\gamma_\kappa - \gamma_\rho)^2}{16\pi^2} V_{ag} V_c \phi_i F(k_{ag}; a) S(k_{ag}; a, \phi_i). \quad (15)$$

In the remaining of the paper, we compute the differential backscattering cross-section $\sigma_{ag} = \sigma_{ag,coh} + \sigma_{ag,inc}$ of an aggregate using Eqs. (5), (11), and (15).

Let us mention that one can derive an alternative expression of the incoherent component of the differential backscattering cross-section based on a Gaussian direct correlation function $\sigma_{ag,inc,G}$ as proposed by Morse and Ingard.[12] The proposed computation of $\sigma_{ag,inc,G}$ is a modified version of the incoherent component of Ref. 12 and is expressed as follows:

$$\sigma_{ag,inc,G}(k) \approx \frac{k_{ag}^4 (\gamma_\kappa - \gamma_\rho)^2}{16\pi^2} V_{ag} \phi_i (1 - \phi_i)$$
$$\times \frac{8\sqrt{2}\pi^{3/2}}{3} d^5 k_{ag}^2 e^{-d^2 k_{ag}}, \quad (16)$$

where d is the correlation distance related to the cell radius a as $d = (2^{1/6}/3^{1/3}\pi^{1/6})a \approx 0.643092 \times a$, as proposed by Insana and Brown [see Eq. (81), p.107, in Ref. 13]. Details can be found in Appendix C. The differential backscattering cross-section of an aggregate based on Eqs. (5), (11), and (16) is denoted $\sigma_{ag,G}$ in the following.

B. Backscatter coefficient BSC_{EMTSFM} from an ensemble of identical aggregates

The BSC from an ensemble of identical aggregates is obtained by summing the contributions from individual effective scatterers and modeling the effective scatterers interaction by a statistical mechanics structure factor S_{ag} as follows:[10,11]

$$BSC_{EMTSFM}(k) = m_{ag}\sigma_{ag}(k)S_{ag}(k; r_{ag}, \phi_{ag}), \quad (17)$$

where m_{ag} is the number density of effective scatterers, which is related to the volume fraction of effective scatterers ϕ_{ag} as $m_{ag} = \phi_{ag}/V_{ag}$ and σ_{ag} is computed using Eqs. (5), (11), and (15). In Eq. (17), S_{ag} is the structure factor for a collection of randomly distributed identical effective scatterers of radius r_{ag} and of concentration ϕ_{ag}, analytically computed as established by Wertheim.[16] The volume fraction of effective scatterers is equal to the volume fraction of cells in the tissue ϕ divided by the aggregate compactness ϕ_i: $\phi_{ag} = \phi/\phi_i$.

III. 3D SIMULATION METHOD

The proposed theory was tested on 3D computer simulations of ultrasound backscatter from aggregating RBCs. The choice of this example was motivated by the fact that RBCs form quasi-spherical aggregates under pathological conditions, as in diabetes mellitus.[6,7] and occupy a large volume fraction (between 30% and 50%), so that the structure factor intervenes. Moreover, in the field of ultrasound blood characterization, RBCs are often assumed to be identical scatterers of simple shape (as spheres) with weak relative acoustic parameter contrast thus allowing to assume the absence of multiple scattering (RBCs $\rho_c = 1.092$ kg/m^3, $\kappa_c = 3.41 \times 10^{-10}$ m/N, and blood plasma $\rho_0 = 1.021$ kg/m^3 and $\kappa_0 = 4.09 \times 10^{-10}$ m/N).[9,11,17]

The 3D simulation study was conducted based on the structure factor model (SFM). The SFM is an ultrasound scattering model largely used to predict the frequency dependence of the BSC from aggregated RBCs.[8,10,11,14,17] The SFM consists of summing contributions from individual cells and modeling cell interaction by a statistical mechanics structure factor, whatever the complexity of the cells spatial distribution such as cell aggregates. The structure factor computation for a complex particle spatial distribution was described in details in Sec. 6.3.1 of Ref. 17. The current section focuses on the procedure for obtaining cell aggregates in the computer simulations, and then on the simulation of the differential backscattering cross section of one cell aggregate, denoted $\sigma_{ag,sim}$, and of the BSC$_{sim}$ from aggregated cells based on the SFM.

A. Simulation of spatial distribution of cells within one aggregate

We describe here how the cell distribution inside one aggregate was computed. The cell particle radius a was set to $2.75\,\mu m$ for all simulations, which corresponds to the RBC size usually used in blood computer simulations.[11] We specified the aggregate radius r_{ag} defined as the radius of the external envelope (Fig. 1) and the aggregate compactness ϕ_i that fixes the number of cells N within the aggregate. N cells were uniformly randomly distributed such that cells within a radius of r_{ag} could overlap, and the total number of overlapping pairs was counted. Then, the system was able to evolve by randomly selecting a cell, and moving it randomly to a new position inside the spherical aggregate. If the number of overlapping pairs of the new system was no more than in the previous system, the displacement was accepted. This procedure was iterated until no overlapping was detected. One can refer to Sec. B.1 in Ref. 18 for more details. This process allowed to reach aggregate compactness ϕ_i up to 40% in 3D, whereas a method using a random sequential absorption[19] would give compactness near 30%. Figure 1 illustrates spatial arrangements of cells within a single aggregate for two aggregate compactnesses of 10% and 40% with an identical aggregate radius $r_{ag}/a = 7$. The radius of gyration was computed using Eq. (9). For the aggregate example given in Fig. 1, a change of compactness from 10% to 40% induces a slight increase of the radius of gyration from $R_g = 13.47\,\mu m$ to $R_g = 14.26\,\mu m$.
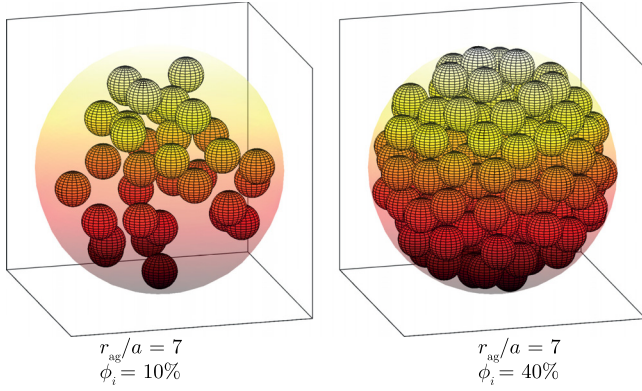
FIG. 1. (Color online) Examples of two cell aggregates of radius $r_{ag}/a = 7$, on the left with a compactness of $\phi_i = 10\%$, and on the right with a compactness of $\phi_i = 40\%$. The radius of the external envelope is displayed with transparency.

B. Computation of a simulated $\sigma_{\rm ag,sim}$ curve

The simulated differential backscattering cross section of one cell aggregate $\sigma_{\rm ag,sim}$, was computed using the SFM (Refs. 10 and 11) as follows:

$$\sigma_{\rm ag,sim}(k) = N\sigma_b(k)S'_{\rm sim}(k), \qquad (18)$$

where σ_b is the differential backscattering cross section of a single cell given by the fluid-filled sphere expression[12,13]

$$\sigma_b(k) = \frac{k^4 V_c^2 \gamma_z^2}{4\pi^2} F(k;a), \qquad (19)$$

and $S'_{\rm sim}$ is the simulated structure factor representing the spatial positioning of the cells inside the aggregate and defined as

$$S'_{\rm sim}(k) = \left\langle \frac{1}{N} \left| \sum_{j=1}^{N} e^{2ik\mathbf{n}_0 \cdot \mathbf{r}_j} \right|^2 \right\rangle, \qquad (20)$$

where the cell positions $\mathbf{r}_j$ are given using the procedure described in Sec. III A. The simulated structure factor $S'_{\rm sim}$

was determined from the 3D Fourier transform of the spatial distribution of cells.[17] A mean $\sigma_{\rm ag,sim}$ curve was computed by averaging over several realizations. To determine the optimum number of realizations, the differential cross-section of one aggregate $\sigma_{\rm ag,sim}$ was computed by averaging over 1, 10, 50, or 100 realizations. Then, in order to study the variation among several differential cross-section simulations $\sigma_{\rm ag,sim}$, ten such simulations of $\sigma_{\rm ag,sim}$ were produced (each one based on 1, 10, 50, or 100 realizations) yielding a mean value $\sigma'_{\rm ag,sim}$ and a standard-deviation over the 10 simulations. Figure 2(a) shows an example of $\sigma'_{\rm ag,sim}$ as a function of frequency for a single aggregate of radius $r_{\rm ag}/a = 6$ and compactness $\phi_i = 30\%$, and the displayed standard deviations quantify the variation over the ten estimates of $\sigma_{\rm ag,sim}$. When using 50 realizations, the coefficients of variation (i.e., the standard-deviation-to-mean ratio) was typically comprised between 1/30 and 1/10 above 40 MHz and was less than 1/100 below 20 MHz. It is clear from Fig. 2(a) that 50 realizations were sufficient to capture the behavior of the $\sigma_{\rm ag,sim}$ curve at high frequencies well.

C. Computation of a simulated *BSC* from several aggregates

Random distributions of non-overlapping aggregates were computed within the simulated cubical volume 480^3 μm^3 by specifying the volume fraction ϕ of cells of radius a, the aggregate radius $r_{\rm ag}$, and the aggregate compactness ϕ_i. The spatial distribution of cells inside each aggregate was performed using the procedure described in Sec. III A. The simulated cubical volume was periodized, i.e., interactions between aggregates were determined under periodic boundary conditions, in order to remove the edge effects. The BSC from aggregated cells was then computed using the SFM as follows:

$$\mathrm{BSC}_{\rm sim}(k) = \frac{\phi}{V_c} \sigma_b(k) S_{\rm sim}(k), \qquad (21)$$

where $S_{\rm sim}$ is the simulated structure factor representing the spatial positioning of the cells inside the simulated tissue.
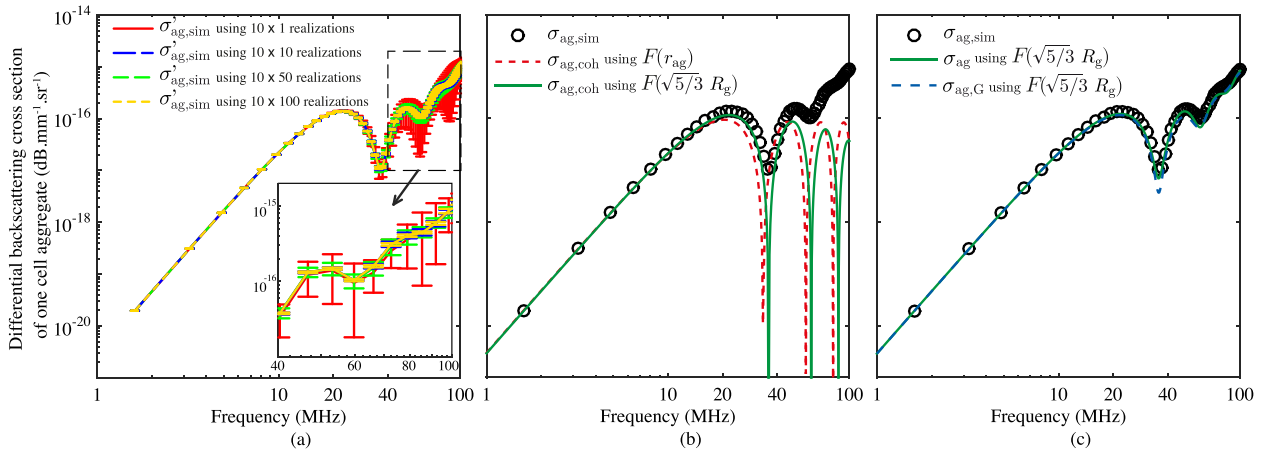

FIG. 2. (Color online) Differential backscattering cross section of one cell aggregate of radius $r_{\rm ag}/a = 6$ and compactness $\phi_i = 30\%$. The symbols represent the $\sigma_{\rm ag,sim}$ computation. (a) Mean value $\sigma'_{\rm ag,sim}$, as a function of frequency, over 10 estimates of $\sigma_{\rm ag,sim}$, each one based on 1, 10, 50, or 100 realizations. The vertical lines indicate ± 1 standard-deviation. (b) The dashed line (or the solid line, respectively) represents the theoretical coherent component $\sigma_{\rm ag,coh}$ given in Eq. (11) using $F(r_{\rm ag})$ [or $F(\sqrt{5/3}R_{\rm g})$, respectively]. (c) The solid line (or the dashed line, respectively) represents the theoretical $\sigma_{\rm ag}$ (or $\sigma_{\rm ag,G}$, respectively), both using $F(\sqrt{5/3}R_{\rm g})$ in the coherent component.

For each distribution of cells, the 3D Fourier transform of the cell spatial positioning was computed to obtain the simulated structure factor.[17] The mean $\mathrm{BSC_{sim}}$ curve was obtained by averaging over 100 realizations for averaging purposes.

IV. RESULTS

A. Comparison of the simulated and theoretical σ_{ag}

The frequency-dependent differential backscattering cross section of one cell aggregate $\sigma_{\mathrm{ag,sim}}$ computed with the SFM (using 50 realizations) is given in Figs. 2(b) and 2(c) for a single aggregate of radius $r_{\mathrm{ag}}/a = 6$ and of compactness $\phi_i = 30\%$. Also shown in Fig. 2(b) [and Fig. 2(c), respectively] are the theoretical differential backscattering cross section considering only the coherent component (and considering both coherent and incoherent components, respectively). In Fig. 2(b), the dashed line (or the solid line, respectively) represents the theoretical $\sigma_{\mathrm{ag,coh}}$ given in Eq. (11) using $F(r_{\mathrm{ag}})$ [or $F(\sqrt{5/3}R_g)$, respectively]. The first peaks of $\sigma_{\mathrm{ag,sim}}$ and $\sigma_{\mathrm{ag,coh}}$ using $F(\sqrt{5/3}R_g)$ occur at the same frequency (approximately 22.1 MHz). On the other hand, the first peak of $\sigma_{\mathrm{ag,coh}}$ using $F(r_{\mathrm{ag}})$ does not match perfectly the simulation and occurs at a lower frequency around 20.5 MHz.

In Fig. 2(c), the solid line represents $\sigma_{\mathrm{ag}} = \sigma_{\mathrm{ag,coh}} + \sigma_{\mathrm{ag,inc}}$ using Eqs. (5), (11), and (15) and the dashed line represents $\sigma_{\mathrm{ag,G}} = \sigma_{\mathrm{ag,coh}} + \sigma_{\mathrm{ag,inc,G}}$ using Eqs. (5), (11), and (16). Consideration of the incoherent component allowed to better match the frequency dependence and amplitude of $\sigma_{\mathrm{ag,sim}}$ at higher frequencies, for either expression $\sigma_{\mathrm{ag,inc}}$ or $\sigma_{\mathrm{ag,inc,G}}$ of the incoherent component. Indeed, the $\sigma_{\mathrm{ag,coh}}$ curve shows very deep dips [Fig. 2(b)], whereas both σ_{ag} and $\sigma_{\mathrm{ag,G}}$ curves match much better the dip behavior of the $\sigma_{\mathrm{ag,sim}}$ curve.

Figure 3 represents the simulated $\sigma_{\mathrm{ag,sim}}$ (symbols) for a radius $r_{\mathrm{ag}}/a = 6$ and aggregate compactnesses $\phi_i = 10\%$, 20%, 30%, and 40%. One can note that the $\sigma_{\mathrm{ag,sim}}$ curves have more pronounced frequency dips when the aggregate compactness increases. For the lower aggregate compactness, only the first peak is well pronounced and the first dip is smooth, whereas the first two peaks and the first dip are

clearly enhanced for the higher aggregate compactnesses. This behavior suggests that for compact aggregates, the incident wave tends to be scattered as if the aggregate was a well-defined sphere, whereas for the lower aggregate compactness, the boundaries of the aggregates are not well defined. The occurrence of the first frequency peak also shifts toward higher frequencies from 22.6 MHz to 25.8 MHz when the aggregate compactness decreases from 40% to 10%. Also represented in Fig. 3 are the theoretical σ_{ag} (solid line) and $\sigma_{\mathrm{ag,G}}$ (dashed line). Both models are accurate at $\phi_i = 30\%$. The $\sigma_{\mathrm{ag,G}}$ curve matches better the simulation results for the highest aggregate compactness $\phi_i = 40\%$, whereas the σ_{ag} curve matches better the two lower compactnesses $\phi_i = 10\%$ and 20%.

The relative errors for theoretical σ_{ag} were evaluated as $\epsilon_R = (\sigma_{\mathrm{ag}} - \sigma_{\mathrm{ag,sim}})/\sigma_{\mathrm{ag,sim}}$, where $\sigma_{\mathrm{ag,sim}}$ was assumed to be the exact solution. Some examples of relative errors for theoretical σ_{ag} are given in Fig. 4(a) for a radius $r_{\mathrm{ag}}/a = 6$ and aggregate compactness $\phi_i = 30\%$ (the aggregating configuration chosen in this example corresponds to the one of Fig. 2). For aggregate compactnesses of 10% and 40%, the relative errors were studied for r_{ag}/a values varying from 5 to 9. In each case, the frequency limit f and the corresponding product kr_{ag} for which the relative error was less than 15% were determined. The resulting product kr_{ag} limits are summarized in Fig. 4(b) and 4(c). First, we assess the improvement of the kr_{ag} for the $\sigma_{\mathrm{ag,coh}}$ expression using $F(\sqrt{5/3}R_g)$ (see the solid curves in Fig. 4). The former modeling using $F(r_{\mathrm{ag}})$ gives kr_{ag} around 0.96 [against 1.63 with the modeling using $F(\sqrt{5/3}R_g)$] for $\phi_i = 10\%$ and around 1.11 [against 1.67 with the modeling using $F(\sqrt{5/3}R_g)$] on average for $\phi_i = 40\%$. Second, we focus on the improvement of the kr_{ag} considering the incoherent component expressions (see the dashed curves in Fig. 4). For the lowest aggregate compactness of 10%, consideration of the incoherent component based on the structure factor $\sigma_{\mathrm{ag,inc}}$ allowed us to increase the kr_{ag} from 1.63 to 2.07, whereas the incoherent component based on the Gaussian direct correlation function $\sigma_{\mathrm{ag,inc,G}}$ did not allow us to improve the kr_{ag} limit. For the highest aggregate compactness of 40%, there was no significant improvement in the kr_{ag} limit whether the incoherent component was considered or not: it means that the kr_{ag}
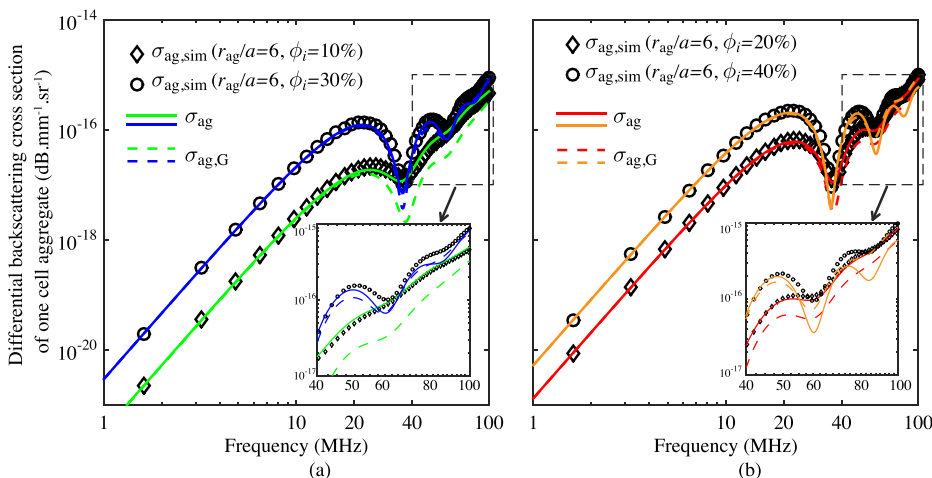

FIG. 3. (Color online) Differential backscattering cross sections of one cell aggregate for different aggregate compactnesses. The symbols represent the $\sigma_{\mathrm{ag,sim}}$ computation. The solid line (dashed line, respectively) represents the theoretical σ_{ag} using Eqs. (5), (11), and (15) [or the theoretical $\sigma_{\mathrm{ag,G}}$ using Eqs. (5), (11), and (16), respectively]. The inner frame of each subfigure shows an enlarged view of the high frequency domain, for more details.
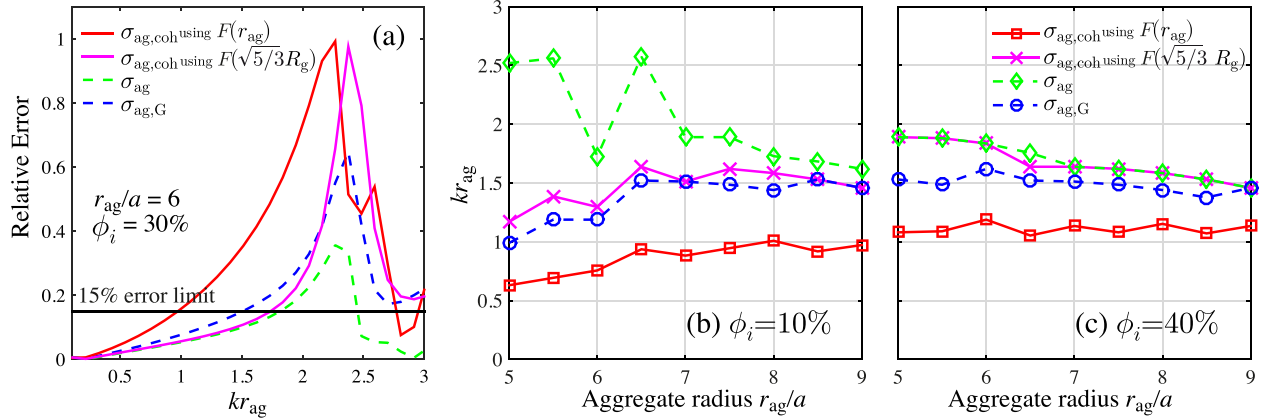
FIG. 4. (Color online) (a) Relative errors for the various theoretical σ_{ag} as a function of kr_{ag} [relative error $= (\sigma_{ag,theo} - \sigma_{ag,sim})/\sigma_{ag,sim}$]. This example shows a radius $r_{ag}/a = 6$ and aggregate compactnesses $\phi_i = 30\%$, as in Fig. 2. (b), (c) Averaged kr_{ag}, as a function of the aggregate size ranging for $r_{ag}/a = 5$–9, for two compactnesses $\phi_i = 10\%$ (b) and $\phi_i = 40\%$ (c). The solid lines correspond to the limits of $\sigma_{ag,coh}$ computed using $F(\sqrt{5/3}R_g)$ (crosses) and using $F(r_{ag})$ (squares). The dotted lines correspond to the limits of σ_{ag} (diamonds) and $\sigma_{ag,G}$ (circles), both computed using the modification of the radius in $F(\sqrt{5/3}R_g)$. Note that the curves marked with crosses and diamonds are superimposed in (c).

increase is mainly due to the modification of $F(\sqrt{5/3}R_g)$ in the coherent component. To conclude, the overall best results are obtained by taking into account (1) the modification of $F(\sqrt{5/3}R_g)$ in the coherent component, and (2) the incoherent component based on the structure factor $\sigma_{ag,inc}$. Thus, for the results presented in the remaining of the paper, we will use the differential backscattering cross section σ_{ag} computed with Eqs. (5), (11), and (15).

B. Comparison of the simulated and theoretical BSC

Figure 5(a) shows simulated and theoretical frequency dependent BSCs for three aggregate sizes $r_{ag}/a = 5$, 7, and 9, a fixed aggregate compactness $\phi_i = 40\%$, and a fixed cell volume fraction $\phi = 16\%$. The symbols represent the BSC_{sim} computed with the SFM. The solid and dashed lines depict the BSC_{EMTSFM} using the proposed model of Eqs. (5), (11), (15), and (17). The theoretical BSC_{EMTSFM} matches well the simulated BSC_{sim}, especially for the amplitude and the frequency occurrence of the first two peaks and dips, whatever the aggregate size considered in this work. In Fig. 5(b) are shown simulated and theoretical BSCs for three aggregate compactnesses $\phi_i = 10\%$, 25%, and 40%, at a

lower $\phi = 4\%$, and a fixed aggregate radius of $r_{ag}/a = 7$. Note that for the study of the aggregate compactness variation, we limit the total cell volume fraction to $\phi = 4\%$ and the lower aggregate compactness to $\phi_i = 10\%$ (corresponding to a value $\phi_{ag} = 40\%$), because the maximum volume fraction of aggregates achievable in computer simulation is approximately 40% using the method described Sec. III.

V. DISCUSSION

A. On the use of simple spatial distribution of cells

The method used in this study to obtain the cell spatial distribution was not based on a generic physical model of interactions between cells. Rather, we used a simple and fast method to generate hundreds of simulated media with a large scale ratio between the cell size ($2.75\,\mu m$) and the whole medium size ($480^3\,\mu m^3$). The purpose was to build a controlled medium containing non-overlapping spherical aggregates, all aggregates having the same radius and compactness with a unique cell spatial distribution defined by a structure factor. The main advantage of this method was the possibility to have various aggregate compactnesses with the same size of aggregates, which allowed to demonstrate the role of the
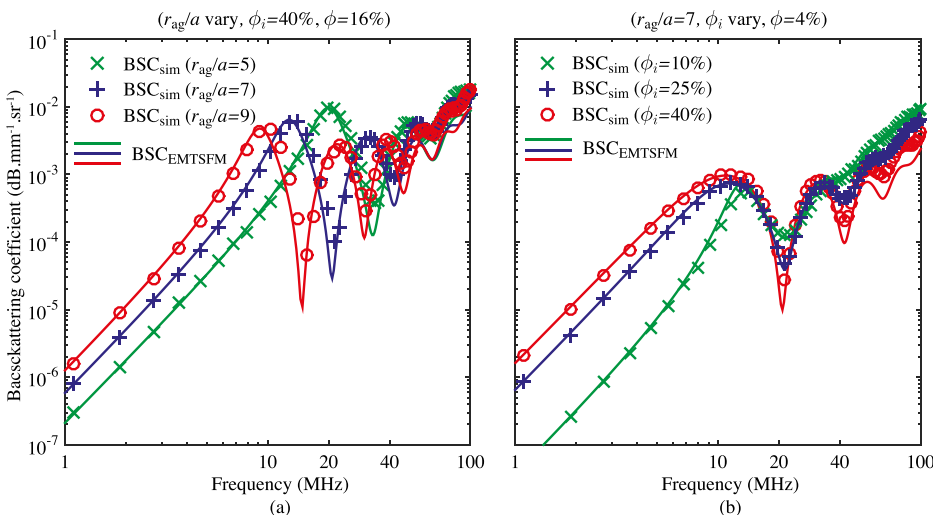

FIG. 5. (Color online) Frequency dependent backscatter coefficients for various aggregate sizes and compactnesses. Symbols represent simulation results and lines represent theoretical BSCs computed using Eq. (17). (a) The volume fraction occupied by the cells in the medium is $\phi = 16\%$ and the aggregate compactness is fixed to $\phi_i = 40\%$. Radii of aggregates vary from $r_{ag}/a = 5$ to $r_{ag}/a = 9$. (b) The volume fraction occupied by the cells in the medium is $\phi = 4\%$ and the aggregate size is fixed to $r_{ag}/a = 7$. Aggregate compactnesses vary from $\phi_i = 10\%$ to $\phi_i = 40\%$.

incoherent scattering component on the BSC frequency dependence at high frequencies. Indeed, the $\sigma_{ag,sim}$ curves had well pronounced peaks and dips for the higher aggregate compactnesses, whereas the first peak was well enhanced and the first dip was smooth for the lower aggregate compactness (see Fig. 3). Theoretical predictions of the σ_{ag} based on the structure factor for the incoherent component proposed in Eq. (15) agreed well with the simulations and validated the proposed theoretical modeling.

In the 3D computer simulations of this study, we had to limit the total volume fraction of cells to a maximum of 16%. Indeed, the procedure we chose to distribute the cells within aggregates allowed reaching a maximum aggregate compactness $\phi_{i,max}$ of 40%. The upper limit of 40% is easily understandable because placing non-deformable identical spheres randomly enough inside a larger sphere without overlapping is not straightforward. In comparison, a standard method using a random sequential absorption[19] would give a compactness close to 30%. The maximum aggregate volume fraction $\phi_{ag,max}$ was thus also fixed to 40%. As a consequence, the maximum value of the total volume fraction ϕ_{max} was limited to $\phi_{max} = \phi_{i,max}\phi_{ag,max} = (40\%)^2 = 16\%$.

B. Variation of the spectral slope

It is interesting to note that, when considering the same aggregate size $r_{ag}/a = 7$ and aggregate compactness $\phi_i = 40\%$ with different volume fractions of $\phi = 16\%$ [see the blue curve in Fig. 5(a)] and $\phi = 4\%$ [see the red curve in Fig. 5(b)], the frequency dependence of the BSC curves is very different. More specifically, we consider the spectral slope (i.e., the linear slope of the BSC as a function of frequency in a log-log scale) of the BSC_{sim} curves before the first peak occurrence. For the aggregating conditions $\phi = 4\%$, $\phi_i = 40\%$ (corresponding to $\phi_{ag} = \phi/\phi_i = 10\%$) [see the red curve in Fig. 5(b)], the BSC_{sim} curve shows a fourth power frequency-dependence (i.e., a spectral slope of 4). However, the spectral slope increases above 4 for the BSC_{sim} curves with aggregating conditions $\phi = 16\%$, $\phi_i = 40\%$ (corresponding to $\phi_{ag} = \phi/\phi_i = 40\%$) presented in Fig. 5(a) and with aggregating conditions $\phi = 4\%$, $\phi_i = 10\%$ (corresponding to $\phi_{ag} = \phi/\phi_i = 40\%$) [see the green curve in Fig. 5(b)]. Considering the theoretical modeling with the EMTSFM, the structure factor S_{ag} causes this increase in the spectral slope, since it models the spectral behavior of the effective scatterer spatial distributions. Indeed, for the product $ka < 1.5$, the structure factor S_{ag} increases with frequency, and the more the aggregate concentration ϕ_{ag} increases, the larger is the increase in the structure factor (see examples of structure factor curves for different volume fractions in Fig. 14 of Ref. 21). The increase in spectral slope with an increase in volume fraction, which could be observed in the current study, is consistent with an earlier 2D numerical study.[10] In this 2D study, the spectral slope was equal to 3 for disaggregated RBCs, as expected using Rayleigh theory in 2D, and when RBCs were aggregated, the spectral slope increased above 3 for volume fractions of 20% and 30%, corresponding to an aggregate with a volume fraction ϕ_{ag} greater than 33% (see Fig. 8 in Ref. 10). Moreover, *in vitro* Couette flow experiments performed by Yu and Cloutier[9] showed spectral slopes that were greater than 4 (at frequencies ranging between 9 and 15 MHz) for shear rates of 2 and $10\,s^{-1}$ at a cell volume fraction of 40% [see Fig. 4(b) in Ref. 9].

C. The benefit of considering the incoherent component

A new theoretical modeling of the differential backscattering cross section from a single cell aggregate was developed in this work and consisted in taking into account a coherent component and an incoherent component in the expression of σ_{ag}. This modeling was compared to numerical simulations based on the SFM. Concerning the coherent component, a slight modification of the $\sigma_{ag,coh}$ expression using $F(\sqrt{5/3}R_g)$ was proposed and allowed the EMT model to better match the frequency occurrences of the first peak and dip observed in simulations [namely, the kr_{ag} limit increased from 1 to 1.6 when considering $F(\sqrt{5/3}R_g)$—see Fig. 4]. Concerning the incoherent component, two expressions of $\sigma_{ag,inc}$ based on the structure factor and on a Gaussian direct correlation function proposed by Morse and Ingard[12] were compared. The numerical study demonstrated the superiority of the formulation using the structure factor over that with the Gaussian direct correlation function, regarding the kr_{ag} study of Fig. 4. The consideration of the incoherent component $\sigma_{ag,inc}$ based on the structure factor allowed to approximate the simulations satisfactorily for an average kr_{ag} around 2 (on average over all the simulations performed), against a kr_{ag} around 1 with the former model considering only the coherent component.

In previous works,[13,20] a decomposition of the differential scattering cross-section into coherent and incoherent terms was presented (pp. 100, 101 in Ref. 13), which is consistent with the one presented here. However, in these works,[13,20] only the case where scatterers are randomly and independently distributed and the coherent term is negligible was considered. In the present study, the coherent component was not negligible, nor was the incoherent one at higher frequencies. Moreover, the proposed model takes into account spatial organization of cells within aggregates, as well as spatial organization of aggregates within surrounding medium.

It is interesting to observe that the simulated $\sigma_{ag,sim}$ curves showed a fourth power frequency dependence (Rayleigh scattering) before the first peak occurrence (see Figs. 2 and 3). When the aggregate compactness varied (Fig. 3), the $\sigma_{ag,sim}$ frequency dependence differed mainly at high frequencies after the first peak. To better understand this high frequency behavior, we analyzed the theoretical respective influence of each scattering component (coherent and incoherent) on the σ_{ag} behavior, while varying the aggregate compactness. According to Eqs. (11) and (15), the σ_{ag} frequency dependence is mainly determined by the fluid-sphere form factor from an effective sphere $F(\sqrt{5/3}R_g)$ that intervenes in the coherent component, and the structure factor $S(a, \phi_i)$ that intervenes in the incoherent component. As shown in Fig. 6(a), an increase in compactness induced a decrease in the structure factor amplitude $S(k; a, \phi_i)$ in the studied frequency bandwidth of 1–100 MHz, and a slight shift toward lower frequencies of the form factor $F(k; r'_{ag})$ peaks and dips. In
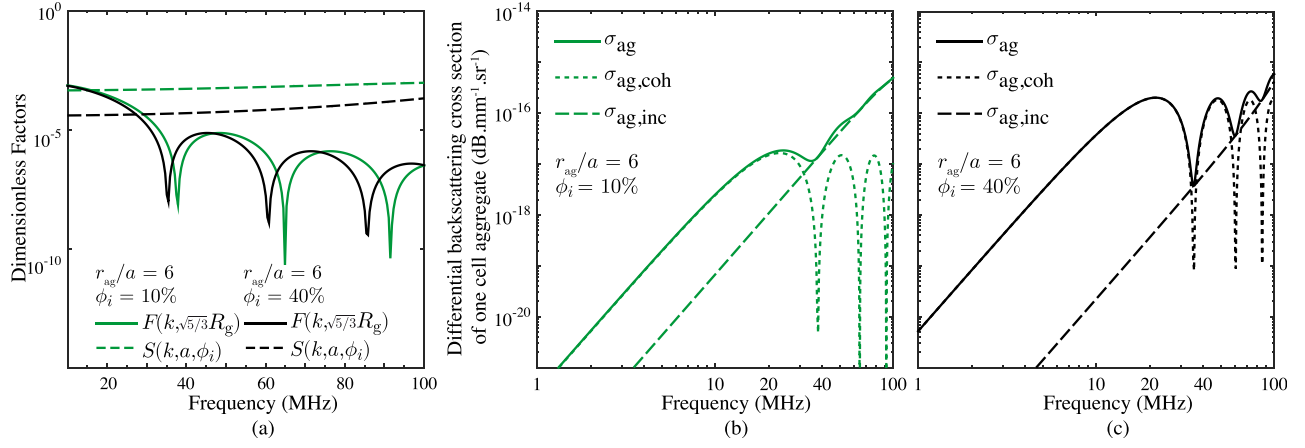
FIG. 6. (Color online) (a) Theoretical form factor $F(k; \sqrt{5/3}R_g)$ and structure factor $S(k; a, \phi_i)$ computed as a function of the frequency for two compactnesses $\phi = 10\%$ and $\phi_i = 40\%$ and aggregate size $r_{ag}/a = 6$. (b), (c) Theoretical differential backscattering cross sections of one cell aggregate σ_{ag}, its coherent component $\sigma_{ag,coh}$, and incoherent component $\sigma_{ag,inc}$, as a function of frequency.

Fig. 6(b) [or Fig. 6(c), respectively] are plotted the theoretical backscattering cross sections (solid lines), the corresponding coherent component $\sigma_{ag,coh}$ (dashed lines), and incoherent component $\sigma_{ag,inc}$ (dotted lines) as defined in Eq. (5), for the same aggregating condition with $r_{ag}/a = 6$ and $\phi_i = 10\%$ (or $\phi_i = 40\%$, respectively). The relative influence of the incoherent component is more important for lower aggregate compactnesses, giving rise to smoother peaks and dips. Also, the frequency shift of the peaks and dips observed in the simulations can be explained theoretically by a dependence of the form factor $F(\sqrt{5/3}R_g)$ on the aggregate compactness. Indeed, the gyration radius value depends on the aggregate compactness as mentioned in Sec. III A. In the framework of an inverse problem approach, it would be useful to approximate the gyration radius as a function of the radius r_{ag} of the aggregate envelope and the aggregate compactness ϕ_i. Based on the 3D building of isotropic aggregates using the method described in Sec. III A, the relationship between R_g, r_{ag}, and ϕ_i was empirically determined as follows:

$$R_g \approx \sqrt{3/5}(r_{ag} + 4.10 \times 10^{-6}\phi_i - 2.34 \times 10^{-6}). \quad (22)$$

This approximation, obtained from a linear regression analysis, shows less than 5% relative error for all tested radii r_{ag}/a (varying from 4 to 9) and compactnesses (varying from 5% to 40%). The estimated R-squared value and p-value were 0.999 and 1.61×10^{-129} respectively.

D. Assumptions and uses of the EMT

The present work allowed a fundamental study to improve modeling of differential backscattering cross-section of one aggregate (or BSC) and to progress in the understanding of the influence of aggregate compactness and size on the BSC. One can question the practical value of this model that assumes spherical aggregates for *in vivo* estimation. In the case of human blood, the assumption of spherical aggregates in the EMT modeling is valid as far as pathological cases are considered. Indeed, as the binding energy between RBCs increases with inflammation,[22] RBC aggregates form clump structures such as in diabetes mellitus.[6,7] However,

aggregates of cells may form irregular shapes like ellipsoids (especially for normal blood). In the case of randomly oriented monodisperse ellipsoids, the frequency occurrence of peaks and dips of σ_{ag} from such structure would likely be in good agreement with those obtained from spheres using the EMT model. To confirm this hypothesis, Fig. 7 shows examples of theoretical form factors for randomly oriented monodisperse ellipsoids (characterized by three radii a, b, and c) as a function of the product ka (a being the characteristic size of the object). The form factors were computed theoretically as in Ref. 23. In Fig. 7, solid lines represent form factors for prolate ellipsoids [radii a, $b = (3/4)a$, $c = (3/4)a$] and oblate ellipsoids [radii a, $b = (4/3)a$, $c = (4/3)a$], and dashed lines represent the corresponding form factors for fluid spheres having the same volume as the ellipsoids (and characterized by a radius r_s). For these ellipsoid dimensions,
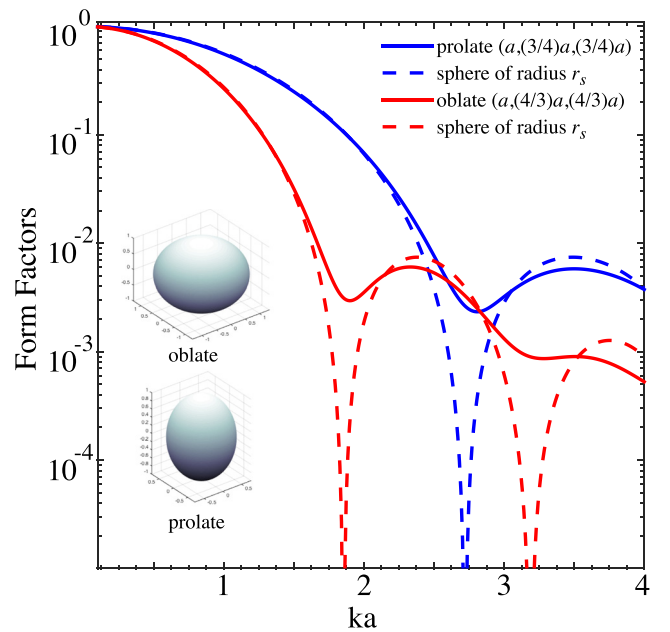

FIG. 7. (Color online) Theoretical form factors of ellipsoids characterized by three radii a, b, and c (solid lines), and spheres (of radius r_s) having the same volume as the ellipsoids (dashed lines) as a function of the product ka (a being characteristic size of the object).

J. Acoust. Soc. Am. **140** (3), September 2016

de Monchy *et al.*   2181

the frequency occurrence of peaks and dips of the form factor from ellipsoids is in good agreement with those obtained from spheres having the same volume. However, the magnitude of the dips of the equivalent sphere form factor is smaller. In the case of ellipsoids oriented in the same direction (such as in the case of normal human rouleaux of RBCs oriented in the blood flow), if the EMT is directly applied to estimate structural parameters such as the aggregate compactness and size, the assumption of spherical shapes would probably create a bias against the parameter estimation.

Finally, QUS techniques for determining tissue microstructure parameters are often based on scattering models (such as the SFM or the EMTSFM studied here) assuming absence of multiple scattering (Born approximation). This is valid in the case of blood scattering because of the low contrast in density and compressibility between RBCs and the surrounding plasma. Nevertheless, one could question the impact of ignoring multiple scattering. Doyle *et al.*[24] simulated multiple scattering between cells for uniform and aggregated cell distributions. Comparison between multiple and simple scattering simulations from the same tissues demonstrated that multiple scattering became significant on the ultrasound backscatter spectra above 60 MHz for uniform cell distributions and above 45 MHz for aggregated cell distributions (see Fig. 13 in Ref. 24). Franceschini *et al.*[25] simulated ultrasonic propagation through RBCs using a time-domain numerical method that has the advantages of requiring no physical approximation (i.e., automatically accounting for multiple scattering). Excellent agreements were obtained between the backscattering responses computed with the time-domain numerical method and with the theoretical SFM in the frequency bandwidth ranging from 10 to 40 MHz (see Fig. 4 in Ref. 25; in this paper,[25] the term "particle theory approach" was used instead of the term "SFM"). Note that the SFM is based on the Born approximation and allows to model the presence of densely packed scattering sources that introduce correlation between the phases of individually scattered waves. In future work, it would be interesting to determine the accuracy of the SFM on wider ranges of frequency bandwidth and of acoustic parameters for the cells.

VI. CONCLUSION

The EMT was further developed to decompose the differential backscattering cross section of a single cell aggregate into coherent and incoherent components. The coherent component, corresponding to the squared norm of the average wave emerging from the effective scatterer, whose radius depends on the gyration radius of the cell aggregate. An important contribution of this new EMT is the taking into account of the incoherent component based on the structure factor, which allowed to approximate the computer simulations satisfactorily for a product kr_{ag} up to 2.

The EMTSFM assumes that all cells are aggregated and that aggregates are identical and isotropic. Therefore, the BSC behavior obtained in all simulations showed a pronounced first peak. In experimental conditions when insonifying aggregated RBCs surrounding by plasma[9] or aggregates of tumor cells surrounding by extracellular matrix,[26] the BSC behavior was smoother and the peaks were less pronounced. The reason behind this might be that real tissues contain several sizes of aggregates, and since the location of BSC peaks are different for different aggregate populations, a relatively smoother BSC curve can be obtained. Therefore, future improvements should consider incorporating polydispersity in aggregate size and compactness to provide an optimal EMTSFM for the inversion of experimental data.

APPENDIX A

The model underlying Eq. (1) is equivalent to the following expression for the tissue function:

$$\gamma_\kappa(\mathbf{r}_0) - \gamma_\rho(\mathbf{r}_0) = (\gamma_\kappa - \gamma_\rho) \sum_{j=1}^{N} \chi(\mathbf{r}_0 - \mathbf{r}_j), \tag{A1}$$

where $\chi(\mathbf{r}_0) = 1$ inside a sphere $\mathbf{V}_a$ of radius a centered at the origin, and 0 elsewhere.

We then compute based on Eq. (A1),

$$\int_{\mathbf{V}_{ag}} [\gamma_\kappa(\mathbf{r}_0) - \gamma_\rho(\mathbf{r}_0)] e^{2ik\mathbf{n}_0 \cdot \mathbf{r}_0} d^3\mathbf{r}_0$$

$$= \sum_{j=1}^{N} (\gamma_\kappa - \gamma_\rho) \int_{\mathbf{V}_{ag}} \chi(\mathbf{r}_0 - \mathbf{r}_j) e^{2ik\mathbf{n}_0 \cdot \mathbf{r}_0} d^3\mathbf{r}_0.$$

Next, considering the change of variable $\mathbf{r}'_0 = \mathbf{r}_0 - \mathbf{r}_j$, one obtains

$$\int_{\mathbf{V}_{ag}} \chi(\mathbf{r}_0 - \mathbf{r}_j) e^{2ik\mathbf{n}_0 \cdot \mathbf{r}_0} d^3\mathbf{r}_0 = \int_{\mathbf{V}_a} e^{2ik\mathbf{n}_0 \cdot (\mathbf{r}'_0 + \mathbf{r}_j)} d^3\mathbf{r}'_0.$$

Last, since $e^{2ik\mathbf{n}_0 \cdot (\mathbf{r}'_0 + \mathbf{r}_j)} = e^{2ik\mathbf{n}_0 \cdot \mathbf{r}'_0} e^{2ik\mathbf{n}_0 \cdot \mathbf{r}_j}$, one concludes that

$$\int_{\mathbf{V}_{ag}} [\gamma_\kappa(\mathbf{r}_0) - \gamma_\rho(\mathbf{r}_0)] e^{2ik\mathbf{n}_0 \cdot \mathbf{r}_0} d^3\mathbf{r}_0$$

$$= (\gamma_\kappa - \gamma_\rho) \left(\int_{\mathbf{V}_a} e^{2ik\mathbf{n}_0 \cdot \mathbf{r}'_0} d^3\mathbf{r}'_0 \right) \sum_{j=1}^{N} e^{2ik\mathbf{n}_0 \cdot \mathbf{r}_j}$$

$$= (\gamma_\kappa - \gamma_\rho) V_c \left(V_c^{-1} \int_{\mathbf{V}_a} e^{2ik\mathbf{n}_0 \cdot \mathbf{r}'_0} d^3\mathbf{r}'_0 \right) \sum_{j=1}^{N} e^{2ik\mathbf{n}_0 \cdot \mathbf{r}_j}.$$

2182   J. Acoust. Soc. Am. **140** (3), September 2016

de Monchy *et al.*

APPENDIX B

This appendix gives the computation steps to obtain the low frequency approximation of $\mathcal{F}_{\mathrm{coh}}(k) = F_0(k;a) 1/N \sum_{j=1}^{N} \langle e^{2ik\mathbf{n}_0 \cdot \mathbf{r}_j} \rangle$.

First, by assuming centrosymmetric aggregates, one has

$$\frac{1}{N}\sum_{j=1}^{N} \langle e^{2ik\mathbf{n}_0 \cdot \mathbf{r}_j} \rangle = \frac{1}{N}\sum_{j=1}^{N} \langle \cos(2k\,\mathbf{n}_0 \cdot \mathbf{r}_j) \rangle$$

$$= \frac{1}{N}\sum_{j=1}^{N} \left\langle \frac{\sin(2k\,|\mathbf{r}_j|)}{2k\,|\mathbf{r}_j|} \right\rangle$$

$$\approx 1 - \frac{2}{3}k^2 \left\langle \frac{1}{N}\sum_{j=1}^{N} |\mathbf{r}_j|^2 \right\rangle,$$

where the last approximation corresponds to the second order Taylor expansion of the expression. An equivalent approach can be found in Ref. 27, pp. 7 and 8. A second order Taylor expansion of $\mathcal{F}_{\mathrm{coh}}(k)$ thus gives

$$\mathcal{F}_{\mathrm{coh}}(k) \approx 1 - \frac{2}{3}k^2 \left(\frac{3}{5}a^2 + \left\langle \frac{1}{N}\sum_{j=1}^{N} |\mathbf{r}_j|^2 \right\rangle \right)$$

$$= 1 - \frac{2}{3}k^2 R_g^2,$$

by using the definition of R_g given in Eq. (9), and the Taylor expansion of $F_0(k;a)(\approx 1 - \frac{2}{5}k^2 a^2)$. Last, since for the equivalent full sphere of radius r', $F_0(k;r') \approx 1 - \frac{2}{5}k^2 r'^2$, we need $r' = \sqrt{(5/3)}R_g$ in order to match the low frequency approximations of the form factors $\mathcal{F}_{\mathrm{coh}}(k)$ and $F_0(k;r')$.

APPENDIX C

This appendix gives the computation steps to obtain the incoherent component of the differential backscattering cross-section $\sigma_{\mathrm{ag,inc,G}}$ based on a Gaussian direct correlation function as proposed by Morse and Ingard.[12]

First, one has

$$\gamma_{\kappa,\mathrm{ag}}(\mathbf{r}_0) - \gamma_{\rho,\mathrm{ag}}(\mathbf{r}_0) = \chi(\mathbf{r}_0)(\gamma_\kappa - \gamma_\rho),$$

where χ is the characteristic function of the cells: $\chi(\mathbf{r}_0) = 1$ inside cells and $\chi(\mathbf{r}_0) = 0$, otherwise. Moreover, we use the following approximation:

$$\langle \gamma_{\kappa,\mathrm{ag}}(\mathbf{r}_0) - \gamma_{\rho,\mathrm{ag}}(\mathbf{r}_0) \rangle \approx \phi_i(\gamma_\kappa - \gamma_\rho).$$

From there, one obtains the expression

$$\Phi_{\mathrm{ag,inc}}(k) = \Phi_{\mathrm{ag}}(k_{\mathrm{ag}}) - \langle \Phi_{\mathrm{ag}}(k_{\mathrm{ag}}) \rangle$$

$$\approx \frac{k_{\mathrm{ag}}^2}{4\pi} \int_{V_{\mathrm{ag}}} (\gamma_\kappa - \gamma_\rho)(\chi(\mathbf{r}_0) - \phi_i) e^{2ik_{\mathrm{ag}}\mathbf{n}_0 \cdot \mathbf{r}_0}\, d^3\mathbf{r}_0.$$

Note that the function $(\gamma_\kappa - \gamma_\rho)(\chi(\mathbf{r}_0) - \phi_i)$ corresponds to the function δ modified from Ref. 12 [Eq. (8.2.24)]. Therefore, the incoherent component of the differential

backscattering cross-section can be computed using the direct correlation function Υ of the compressibility and density fluctuations as follows:

$$\sigma_{\mathrm{ag,inc}}(k) = \langle |\Phi_{\mathrm{ag,inc}}(k)|^2 \rangle$$

$$\approx \frac{k_{\mathrm{ag}}^4 (\gamma_\kappa - \gamma_\rho)^2}{16\pi^2} V_{\mathrm{ag}} \int_{V_{\mathrm{ag}}} \Upsilon(\Delta\mathbf{r}) e^{2ik_{\mathrm{ag}}\mathbf{n}_0 \cdot \Delta\mathbf{r}}\, d^3\Delta\mathbf{r},$$

(C1)

where

$$\Upsilon(\Delta\mathbf{r}) = \frac{1}{V_{\mathrm{ag}}} \left\langle \int_{V_{\mathrm{ag}}} (\chi(\mathbf{r}_0) - \phi_i)(\chi(\mathbf{r}_0 + \Delta\mathbf{r}) - \phi_i)\, d^3\mathbf{r}_0 \right\rangle.$$

The function Υ depends only on $\Delta r = |\Delta\mathbf{r}|$ and must have the following properties: the mean value of $\Upsilon(\Delta\mathbf{r})$ is zero and $\lim_{|\Delta\mathbf{r}|\to\infty}\Upsilon(\Delta\mathbf{r}) = 0$. Under the postulate of a Gaussian model, the expression of the direct correlation function Υ is given by Morse and Ingard,[12] Eq. (8.2.26),

$$\Upsilon(\Delta r) \approx \Upsilon(0)\left(1 - \frac{\Delta r^2}{3d^2}\right) e^{-\Delta r^2/(2d^2)},$$

where $\Upsilon(0) = \phi_i(1 - \phi_i)$, and the correlation distance d is related to the cell radius a as $d = (2^{1/6}/3^{1/3}\pi^{1/6})a \approx 0.643092 \times a$ as defined by Insana and Brown,[13] Eq. (81), p. 107. Performing the integral in Eq. (C1), one then obtains the Gaussian incoherent component expressed in Eq. (16).

[1] F. L. Lizzi, M. Astor, T. Liu, C. Deng, D. J. Coleman, and R. H. Silverman, "Ultrasonic spectrum analysis for tissue assays and therapy evaluation," Int. J. Imaging Syst. Technol. **8**, 3–10 (1997).

[2] M. F. Insana, R. F. Wagner, D. G. Brown, and T. J. Hall, "Describing small-scale structure in random media using pulse-echo ultrasound," J. Acoust. Soc. Am. **87**, 179–192 (1990).

[3] R. M. Vlad, R. K. Saha, N. M. Alajez, S. Ranieri, G. J. Czarnota, and M. C. Kolios, "An increase in cellular size variance contributes to the increase in ultrasound backscatter during cell death," Ultrasound Med. Biol. **36**, 1546–1558 (2010).

[4] E. Franceschini, R. Guillermin, F. Tourniaire, S. Roffino, E. Lamy, and J.-F. Landrier, "Structure factor model for understanding the measured backscatter coefficients from concentrated cell pellet biophantoms," J. Acoust. Soc. Am. **135**, 3620–3631 (2014).

[5] M. Oelze and J. F. Zachary, "Examination of cancer in mouse models using high-frequency quantitative ultrasound," Ultrasound Med. Biol. **32**, 1639–1648 (2006).

[6] H. Schmid-Schonbein, G. Gallasch, J. V. Gosen, E. Volger, and H. J. Klose, "Red cell aggregation in blood flow. I. New methods of quantification," Klin. Wschr. **54**, 149–157 (1976).

[7] H. Schmid-Schonbein, H. Malotta, and F. Striesow, "Erythrocyte aggregation: Causes, consequences and methods of assessment," Tijdschr NVKS **15**, 88–97 (1990).

[8] D. Savery and G. Cloutier, "A point process approach to assess the frequency dependence of ultrasound backscattering by aggregating red blood cells," J. Acoust. Soc. Am. **110**, 3252–3262 (2001).

[9] F. T. H. Yu and G. Cloutier, "Experimental ultrasound characterization of red blood cell aggregation using the structure factor size estimator," J. Acoust. Soc. Am. **122**, 645–656 (2007).

[10] E. Franceschini, B. Metzger, and G. Cloutier, "Forward problem study of an effective medium model for ultrasound blood characterization," IEEE Trans. Ultrason. Ferroelectr. Freq. Control **58**, 2668–2679 (2011).

[11] E. Franceschini, R. K. Saha, and G. Cloutier, "Comparison of three scattering models for ultrasound blood characterization," IEEE Trans. Ultrason. Ferroelectr. Freq. Control **60**, 2321–2334 (2013).

J. Acoust. Soc. Am. **140** (3), September 2016

de Monchy et al. 2183

[12]P. M. Morse and K. U. Ingard, *Theoretical Acoustics* (Princeton University Press, Princeton, NJ, 1968), Chap. 8, pp. 400–466.

[13]M. F. Insana and D. G. Brown, "Acoustic scattering theory applied to soft biological tissues," in *Ultrasonic Scattering in Biological Tissues*, edited by K. K. Shung and G. A. Thieme (CRC, Boca Raton, FL, 1993), Chap. 4, pp. 76–124.

[14]R. K. Saha, E. Franceschini, and G. Cloutier, "Assessment of accuracy of the structure-factor-size-estimator method in determining red blood cell aggregate size from ultrasound spectral backscatter coefficient," J. Acoust. Soc. Am. **129**, 2269–2277 (2011).

[15]V. Twersky, "Low-frequency scattering by correlated distributions of randomly oriented particles," J. Acoust. Soc. Am. **81**, 1609–1618 (1987).

[16]M. S. Wertheim, "Exact solution of the Percus-Yevick integral equation for hard spheres," Phys. Rev. Lett. **10**, 321–323 (1963).

[17]E. Franceschini and G. Cloutier, "Modeling of ultrasound backscattering by aggregating red blood cells," in *Quantitative Ultrasound in Soft Tissues*, edited by J. Mamou and M. L. Oelze (Springer, New York, 2013), Chap. 6, pp. 117–146.

[18]R. K. Saha and G. Cloutier, "Monte Carlo study on ultrasound backscattering by three-dimensional distributions of red blood cells," Phys. Rev. E **78**(6), 061919 (2008).

[19]E. L. Hinrichsen, J. Feder, and T. Jossang, "Geometry of random sequential adsorption," J. Stat. Phys. **44**, 793–827 (1986).

[20]J. F. Chen, E. L. Madsen, and J. A. Zagzebski, "A method for determination of frequency-dependent effective scatterer number density," J. Acoust. Soc. Am. **95**, 77–85 (1994).

[21]E. Franceschini and R. Guillermin, "Experimental assessment of four ultrasound scattering models for characterizing concentrated tissue-mimicking phantoms," J. Acoust. Soc. Am. **132**, 3735–3747 (2012).

[22]X. Weng, G. Cloutier, R. Beaulieu, and G. O. Roederer, "Influence of acute-phase proteins on erythrocyte aggregation," Am. J. Physiol. **271**, H2346–H2352 (1996).

[23]L. A. Feigin and D. I. Svergun, *Structure Analysis by Small-Angle X-Ray and Neutron Scattering*, edited by G. W. Taylor (Plenum, New York, 1987), p. 92.

[24]T. E. Doyle, A. T. Tew, K. H. Warnick, and B. L. Carruth, "Simulation of elastic wave scattering in cells and tissues at the microscopic level," J. Acoust. Soc. Am. **125**, 1751–1767 (2009).

[25]E. Franceschini, B. Lombard, and J. Piraux, "Ultrasound characterization of red blood cells distribution: A wave scattering simulation study," J. Phys. Conf. Ser. **269**, 012014 (2011).

[26]A. Han and W. D. O'Brien, "Structure function estimated from histological tissue sections," IEEE Trans. Ultrason. Ferroelectr. Freq. Control **63**(9), 1296–1305 (2016).

[27]A. Guinier, G. Fournet, and K. L. Yudowitch, "General theory," in *Small-Angle Scattering of X-Rays* (Wiley, New York, 1955), Chap. 2, pp. 5–82.